Review of Scientific Instruments

Optical Raman measurements of low frequency magnons under high pressure

Cite as: Rev. Sci. Instrum. **91**, 113902 (2020); https://doi.org/10.1063/5.0026311
Submitted: 23 August 2020 . Accepted: 18 October 2020 . Published Online: 04 November 2020

Xiang Li, S. E. Cooper, A. Krishnadas, D. M. Silevitch, T. F. Rosenbaum, and Yejun Feng

Review of Scientific Instruments ARTICLE scitation.org/journal/rsi

Optical Raman measurements of low frequency magnons under high pressure

Cite as: Rev. Sci. Instrum. 91, 113902 (2020); doi: 10.1063/5.0026311
Submitted: 23 August 2020 • Accepted: 18 October 2020 •
Published Online: 4 November 2020

Xiang Li,[1,2] S. E. Cooper,[2] A. Krishnadas,[2] D. M. Silevitch,[1] T. F. Rosenbaum,[1] and Yejun Feng[1,2,a)]

AFFILIATIONS

[1] Division of Physics, Mathematics, and Astronomy, California Institute of Technology, Pasadena, California 91125, USA
[2] Okinawa Institute of Science and Technology Graduate University, Onna, Okinawa 904-0495, Japan

[a)] **Author to whom correspondence should be addressed:** yejun@oist.jp

ABSTRACT

The application of giga-Pascal scale pressures has been widely used as a tool to systematically tune the properties of materials in order to access such general questions as the driving mechanisms underlying phase transitions. While there is a large and growing set of experimental tools successfully applied to high-pressure environments, the compatibility between diamond anvil cells and optical probes offers further potential for examining lattice, magnetic, and electronic states, along with their excitations. Here, we describe the construction of a highly efficient optical Raman spectrometer that enables measurements of magnetic excitations in single crystals down to energies of 9 cm^{-1} (1.1 meV or 13 K) at cryogenic temperatures and under pressures of tens of GPa.

I. INTRODUCTION

Magnetism and magnetic materials are central topics in a wide range of research fields such as geology, chemistry, materials science, and physics, along with many practical applications, from imaging to information storage. For many of these fields, an athermal tuning mechanism for the magnetic state is a powerful method employed to reveal the underlying energy scales, interactions, ordering, and transitions as the magnetism evolves. Hydrostatic pressure is a preferred technique for such studies as it can drive a change in energy density comparable to that of the magnetic couplings. Many of the standard techniques for probing magnetic ground states and their excitations have been adapted for compatibility with high-pressure environments, including neutron magnetic diffraction,[1] μSR spectroscopy,[2] x-ray magnetic diffraction,[3,4] synchrotron Mössbauer spectroscopy,[5] and x-ray magnetic dichroism.[6] These, however, often require the use of international user facilities. Optical Raman scattering provides a means to explore magnetic excitations under pressure within an individual research laboratory. Moreover, it can offer unique insights into symmetry and local structure.

Optical Raman scattering is capable of probing lattice,[7] magnetic,[8] and electronic[9] degrees of freedom, with correspondingly increasing experimental difficulty. Despite the wide popularity of optical Raman techniques even before the invention of the laser[7] and their application to high pressure sample environments starting soon after the introduction of the diamond anvil cell,[10] existing high-pressure Raman studies have focused primarily on relatively high energies, above 100 cm^{-1}, examining the evolution of lattice phonons and pressure-driven structural transitions. To date, there are only a few examples in the literature[10–17] of Raman scattering at low frequencies (<100 cm^{-1}) and high pressures, thereby permitting measurement of single magnons or charge-density-wave fluctuations.

Here, we describe the construction of an instrument capable of obtaining Raman spectra down to 9 cm^{-1} under multi-GPa pressures and cryogenic temperatures. By carefully designing the optical, cryogenic, and high-pressure components, our Raman probe offers spatial sensitivity, polarization analysis, and a high signal-to-background ratio. It is a highly efficient tool for exploring the evolution of magnetic excitations under pressure.

II. OPTICAL CONFIGURATION

Several groups have described high-pressure Raman systems using a traditional triple-grating spectrometer to collect the spectra.[13–17] The first two stages are combined in a subtraction mode

to remove excessive spectral weight outside the measurement range, and a physical block between the two stages eliminates the elastic laser line. We instead elect to use Bragg-diffraction-based volume grating bandpass and notch filters (BragGrate OD3 or OD4 types, OptiGrate Corp. USA) to focus on the removal of the elastic line. This allows the measurement of the inelastic spectrum much closer to the elastic frequency (within 10 cm^{-1}) and also provides a much higher throughput efficiency compared to the significant photon flux loss through 8–9 reflective mirrors in the first two stages of a triple-grating spectrometer. The tradeoff associated with the use of these volume Bragg gratings is that it essentially entails choosing one specific laser wavelength for the whole system. Changing the wavelength is economically demanding and time consuming as it requires both the purchase of a whole new set of volume Bragg grating bandpass and notch filters specifically for the desired laser wavelength and rearrangement/realignment of large portions of the optical path. Fixing the laser wavelength would prevent studies using resonant Raman scattering. It also rules out the possibility of varying the incident laser wavelength, taking advantage of the changing balance between Raman and fluorescence efficiencies at different wavelengths to improve the signal-to-noise ratio. Nevertheless, for the desired magnetic measurements, the advantage in throughput outweighs the above considerations.

We choose a single-frequency, continuous wave diode-pumped 659.6 nm laser (100-mW, Cobolt AB, Sweden). The long wavelength reduces the Raman efficiency. However, it also significantly reduces the fluorescence, which is advantageous in high pressure measurements as the sample surface is covered by a pressure medium rather than being in vacuum.

The general layout of our optical setup is presented in Fig. 1(a). Along the incident beam path, the laser first passes through a beam expander to generate a relatively constant Gaussian beam profile over a long distance. The intensity, polarization state, and spectral profile of the incident laser beam are shaped by neutral density filters, a quarter wave plate plus a linear polarizer, and volume Bragg grating bandpass filters, respectively.

While the incident and Raman scattered light paths can be chosen independently, here we limit our probe to a backscattering Raman geometry, $\bar{z}(P_1P_2)z$, where $\bar{z}$ and z are the diametrically opposed propagation directions of the incident and back-scattered light and P_1 and P_2 are the polarization states of the incident and scattered photons, respectively. This collinear geometry is dictated by the typical geometry of an opposite-anvil high-pressure diamond anvil cell, and to a lesser extent by the optical window of the cryostat [Fig. 2(a)]. The incident laser path converges with the scattered light path at the first of the five volume Bragg grating notch filters [Fig. 1(a)].

The set of five notch filters in series along the scattered light path rejects elastically scattered laser light that originates from the focused spot on the sample surface. In addition, random scattered light from multiple surfaces and fluorescence along the beam path are rejected by a home-built confocal microscopy structure to further enhance the signal-to-background ratio. After the Raman signal passes through a polarization analyzer to define the detection scheme, the light is fiber-coupled to the entrance of a single-grating spectrometer. We use a single-grating spectrometer of 700-mm or 750-mm length (such as SpectraPro HRS-750 or the third stage of TriVista-557, Princeton Instruments), with three grating choices of 600 lines/mm, 1200 lines/mm, and 1800 lines/mm, to provide a flexible combination of spectral range and resolution. A liquid-nitrogen-cooled CCD camera with 1340 × 400 $pixel^2$ (PyLoN-400BR-eXcelon, Princeton Instruments) serves as a photon detector with low electronic noise and a consistently high quantum efficiency (>90%) in the spectral range between 600 nm and 900 nm.

III. HIGH-PRESSURE CRYOGENIC SAMPLE ENVIRONMENT

Here, we discuss the specific considerations to meet the constraints associated with the high-pressure and low temperature sample environment. The Raman spectrometer was constructed around a commercial microscope objective instead of assembling our own compound lens. We use a 20× microscope lens with an extra-long 25.5 mm working distance [Fig. 2(a)] and a numerical aperture (NA) of 0.40 (M Plan Apo NIR B, Mitutoyo Co., Japan). This lens was designed by the manufacturer to provide a wide range of apochromatic correction from 420 nm to 1064 nm and has achieved a tight focusing spot of ~5 μm lateral size and ~5 μm depth of focus with our optical arrangement. The narrow depth of focus together with the confocal design eases the need for ultrapure diamonds with very low fluorescence; all our data presented here were collected using cells assembled with type I diamond anvils.

To position our micrometer-sized focused laser beam spot on the sample under high pressure, we mount the Raman optical setup and the cryostat on heavy-duty x–y and z translational stages (Models 5102.40 and 5103.C30, Huber Diffraktionstechnik GmbH & Co. KG) [Fig. 1(b)]. All three degrees of movement have a repeatability of about 2 μm as specified by the manufacturer. This fine translational precision allows surveying many different parts of the sample surface to assess potential damage areas, intrinsically heterogeneous phase coexistence (for instance, near a first-order quantum phase transition), or other circumstances where sample heterogeneity is germane. To assist in positioning the focused laser beam on particular locations on the sample, a white-light illuminated CCD camera-based imaging system can be inserted into the beam path while maintaining the presence of the laser beam.

Both the cryostat and the high-pressure cells are constructed to be compatible with the 25.5-mm optical working distance. We use a cryogen-free Gifford–McMahon (GM) cryostat (0.5 W cooling power at 4.2 K, Sumitomo RDK-205E) with an optical window and a thermal radiation shield anchored at the first (60 K) cooling stage. Our pressure cell is directly mounted on the cold finger to optimize the cooling power and typically can be cooled below 4.5 K despite the large surface area of the pressure cell and the optical-access opening on the 60-K radiation shield [Fig. 2(a)]. At $T = 4.5$ K, the pressure cell has a peak-to-peak vibration amplitude of ~13 μm. However, it is in the plane transverse to the incident laser beam, so the vibration does not affect the laser focusing condition on the sample surface. Replacing the GM cryocooler with a pulse-tube based cryocooler would offer both larger cooling power in the range of 1 W–2 W at 4.2 K and a reduction in the vibration amplitude to ~10 μm. The primary effect of the vibration is to increase the effective lateral spot size, which serves to distribute the heat load from the laser over a larger area and thereby reduces the amount of local heating. The cryostat vibration should not affect the detection of

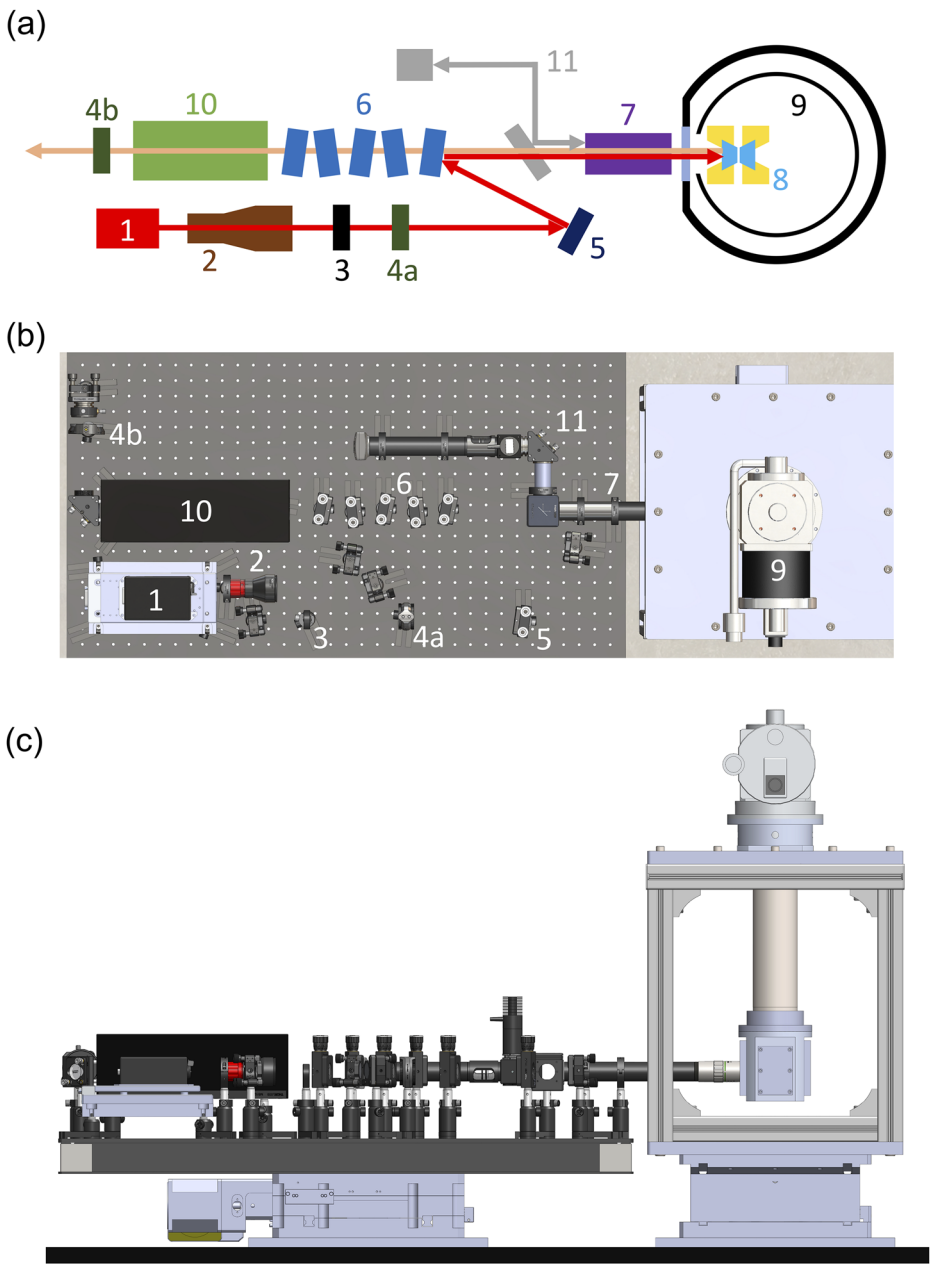

FIG. 1. (a) Optical schematic for the high-pressure Raman instrument. (1) Continuous-wave laser; (2) beam expander; (3) neutral density attenuators; (4a–b) quarter wave plate and polarization analyzers; (5) volume Bragg bandpass filter; (6) volume Bragg notch filters; (7) high-NA long-working distance microscope objective; (8) diamond anvil cell; (9) cryostat with thermal radiation shield; (10) confocal microscopy structure; and (11) white light imaging system. (b) Aerial and (c) side view CAD rendering of the Raman instrument showing the optical bench and cryostat mounted on x–y and z translational stages, respectively. The numerical labels in panel (b) denote the same parts as in panel (a).

coexisting phases and magnetic domains, as long as the vibration amplitude is smaller than the typical high-pressure sample size of 70 μm–200 μm.[4,18,19] While individual domain sizes are not always larger than the focused laser spot, the surface/volume ratio of different domains could vary significantly over the spatial area and as a function of pressure.[20]

We construct our high-pressure diamond anvil cell to have an asymmetric structure to minimize the access distance from one side. While such asymmetric cell designs are well-known in the literature,[10,21] here we have the additional design constraint of incorporating a helium membrane mechanism to allow tuning pressure *in situ* at low temperature.[4,18] We take a modified Merrill–Bassett type three-pin cell design[4] and add an access hole that allows the membrane tubing to pass unconstrained through the cell body after the cell is sealed (Fig. 2), similar to the approach used in a pressure cell designed for the Physical Property Measurement System (Quantum Design, Inc. USA) family of cryostats.[19] By putting all tubing, sealing screws with Belleville washers, and even the thermometer on one side of the pressure cell, we can comfortably construct the vacuum window and radiation shield in the space between

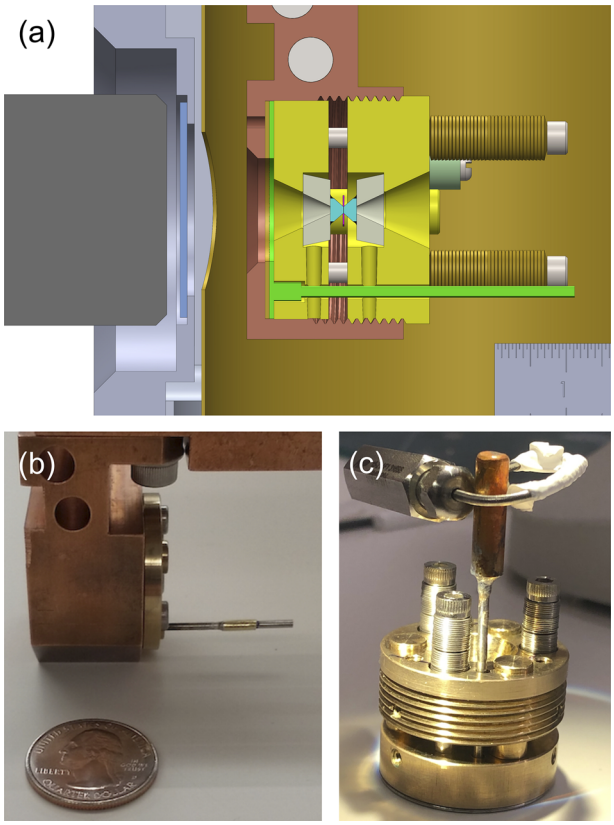

FIG. 2. (a) Side view CAD rendering detailing the environment around the sample at high pressure and cryogenic temperature. From left to right: microscope lens (gray), 1.5 mm-thick fused quartz window on the cryostat (gray blue), brass radiation shield with optical opening (gold), pressure cell cap (red-brown), membrane (fluorescent green), and the high-pressure diamond anvil cell (yellow). The pressure chamber between the anvils is within the working distance of the microscope lens. The membrane line is passed through the cell body toward the back, alongside the sealing screws and Belleville washer stacks. A ruler included in the CAD rendering marks 1 cm. (b) Side view photograph of the pressure cell, helium membrane, and cell cap assembly following the rendering in panel (a). (c) A fully assembled cell with the membrane line lead-soldered to an adaptor for further connection to the regular tubing system.

the microscope lens and the high-pressure cell (Fig. 2) with a couple of millimeters of clearance on both sides of the vacuum window.

The numerical aperture of 0.40 of the microscope lens matches up well with the 1-mm diameter optical opening in the tungsten carbide seats supporting the Drukker type diamond anvils in our pressure cell. Our pressure cells have been constructed with ±25° or ±35° conical angles; both are compatible with the specified numerical aperture.

Since the light path is parallel to the axial direction of the diamond anvils, the restriction to a single probing geometry, $\bar{z}(P_1P_2)z$, might be of concern for non-cubic systems as potentially not all Raman active modes could be explored under high pressure. This issue is most acute for layered materials as typical pressure chambers are disk shaped and the layered samples are often mounted inside the pressure chamber with the naturally cleaving *a*–*b* plane parallel to the diamond culet surface. To overcome this limitation, we employ a culet-perforated diamond anvil design[19,22] to allow mounting plate-like samples on their side inside the perforated diamond cavity. Assuming that the *c*-axis is the stacking axis of *a*–*b* layers, the crystal can be placed with its large *a*–*b* plane surface parallel to the laser beam direction, as shown in Fig. 3. This innovation makes possible the exploration of the pressure evolution of Raman active modes in the *a*–*c* or *b*–*c* planes.

Our general approach to maintaining a highly hydrostatic sample environment has been discussed extensively in the past.[4,18] Here, we follow the parameters listed in Ref. 4 for the initial sample pressure chamber construction. We have considered several possible choices for pressure medium. Our past experience has established that argon is not a sufficiently hydrostatic pressure medium. High pressure loading of supercritical neon[3] or liquid helium in the superfluid state is not easily available, and they do not necessarily maintain a large sample chamber relative to the size of the sample, which is important to sustain hydrostaticity.[18] Here, we have used both a methanol:ethanol 4:1 (ME 4:1) mixture and liquid nitrogen as pressure media. Under pressure and at low temperature, nitrogen has several different phases and many strong vibration modes in

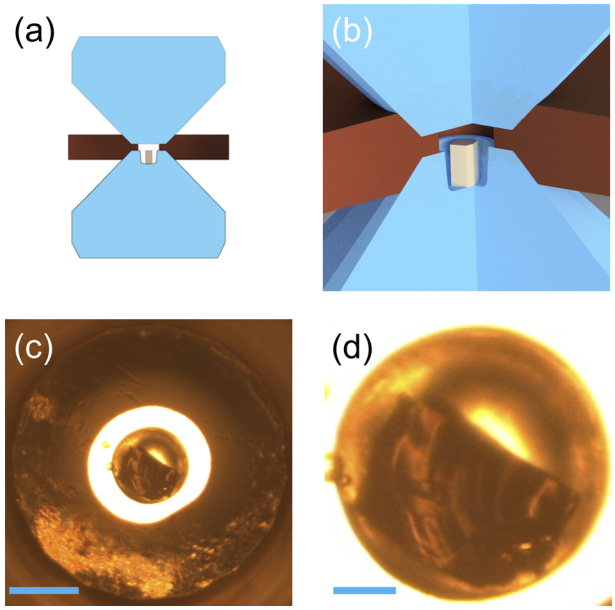

FIG. 3. Culet-perforated diamond anvils for studying Raman modes scattered from the side surface of layered materials. (a) Schematic of the culet-perforated diamond anvil in the high-pressure assembly. The two diamond anvils (blue) sandwich the gasket (brown) and a sample (gray) inside an optically transparent pressure medium, with one of the anvils having a perforation in its culet. (b) Enlarged three-dimensional cut-out view near the sample chamber. (c) Micrograph of a sample in a pressure chamber at 1.8 GPa. Illumination is from below to illustrate the sample chamber enclosed by the metallic gasket and the perforated hole in the middle. A piece of single crystal Sr_2IrO_4 is placed inside the perforated hole, fixed by a tiny amount of Apiezon grease at the bottom. A few ruby balls are placed on the edge of the perforation for *in situ* pressure measurements. The scale bar represents 200 μm. (d) Enlarged view of the sample inside the perforation showing the shining surface condition of a *b*–*c* plane cross section. The parallel edges of the sample are the naturally cleaving *a*–*b* planes of Sr_2IrO_4 on both sides. The scale bar represents 50 μm.

the spectral range between 50 cm^{-1} and 350 cm^{-1},[11,12,23] which can overwhelm the Raman signals of the sample within this range. By contrast, the ME 4:1 mixture has a glassy structure, which provides only a slowly varying and mostly featureless background, with no sharp Raman peaks below 850 cm^{-1}. Both media preserve sample quality, with the sharpest width of lattice (phonon) Raman modes maintained at 11.1 cm^{-1} FWHM at 19.4 GPa with nitrogen and 5.2 cm^{-1} FWHM at 23.5 GPa with ME 4:1, respectively, in our current measurements. By comparison, the sharpest Raman mode in a previous measurement at 10 K using neon as the pressure medium has a 19.4 cm^{-1} FWHM at 29.2 GPa.[3]

IV. RESULTS AND DISCUSSION

We demonstrate the effectiveness of our Raman spectrometer by measuring Sr_2IrO_4 single crystals under pressure. Sr_2IrO_4 has a tetragonal crystal structure and cleaves well along the a–b plane. It has a canted antiferromagnetic ground state with spins mostly projected within the a–b plane but also a small component along the c-axis.[24,25] The low-frequency Raman active magnons are well documented in the literature.[24,25] We test two different sample configurations: one with the a–b plane perpendicular to the laser propagation direction and the other with the b–c plane perpendicular to the laser propagation direction, taking advantage of the culet-perforated diamond anvil design. The measured Raman spectra in the low-frequency regime below 100 cm^{-1} are presented in Fig. 4. Several single-magnon peaks are clearly visible. In the $\bar{c}(ab)c$ configuration, the observed 20 cm^{-1} magnon peak is consistent with the behavior at ambient pressure,[24,25] and the peak is instrument resolution limited with a 2.1 cm^{-1} FWHM at 3.0 GPa, comparable to the best Raman magnon spectra at ambient pressure.[25] The Raman spectrum measured in the $\bar{a}(cb)a$ configuration demonstrates two well-resolved magnons at 25 cm^{-1} and 37 cm^{-1}. These peaks are slightly broadened to 4.8 cm^{-1} FWHM at 4.5 GPa. In comparison, the lattice B_{2g} phonon modes[25] have FWHMs of 4.2 cm^{-1} and 4.6 cm^{-1}(Fig. 4 insets). While the $\bar{c}(ab)c$ and $\bar{a}(cb)a$ configurations likely probe magnon modes in the a–b and b–c planes, respectively, it is possible that the spin correlations along the c-axis direction are not as well defined as those within the a–b plane due to the anisotropic, layered lattice structure.

The diamond anvil is the only optical component under stress in our high-pressure Raman scattering setup. It will deform under high pressure,[21] which raises concerns about strain-induced birefringence. This could affect polarization-sensitive spectroscopy studies under pressure such as second harmonic generation and Raman scattering. Although the intrinsic birefringence from a cubic crystal structure is typically small,[26] real diamonds are known to exhibit optical birefringence at ambient condition due to various types of defects and strain.[27] Fortunately, diamond anvils used in high pressure experiments are generally free of visible inclusions, as well as fractures or ring cracks, two major causes of birefringence.[27] In addition, the birefringence is much more significant with anisotropy in nitrogen-poor type II diamonds,[27] which we do not need to use because of the tight focusing microscope lens and the confocal setup. Finally, our high-pressure sample chambers[4] are constructed significantly larger in size than typical high-pressure assemblies, and the hydrostatic condition significantly reduces large

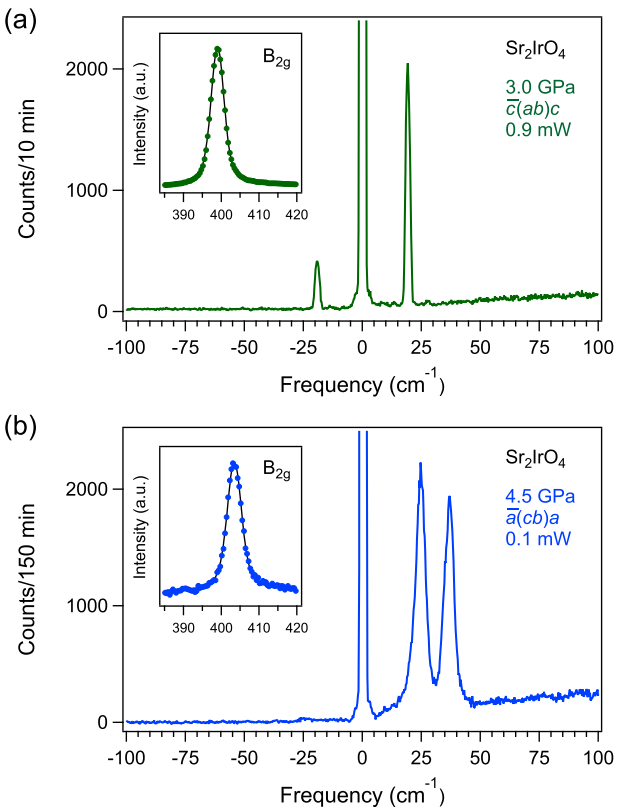

FIG. 4. Representative magnon spectra measured under pressure and at low temperature, using (a) 0.90 mW laser power in the $\bar{c}(ab)c$ configuration and (b) 0.10 mW laser power in the $\bar{a}(cb)a$ configuration. Insets demonstrate the lattice B_{2g} phonon modes[25] probed with a circular-in unpolarized-out configuration at indicated pressures. While the thermometer on the pressure cell typically registers 4.5 K, the sample temperature can be estimated through the Stokes–anti-Stokes intensity ratio to be 17 K and 8.6 K for the two laser power settings, respectively. A further reduction in laser power to 0.05 mW did not noticeably change the intensity ratio.

stress gradients. Judging from polarization selection rules of phonon modes, especially the extinction of the B_{2g} mode (~395 cm^{-1} at ambient pressure, Fig. 4 insets) under the XX polarization configuration,[25] we estimate that the birefringence in our setup causes no more than 1° rotation of the linearly polarized light at 8.0 GPa. More studies are necessary to understand the birefringence effect at higher pressures.

Previous Raman spectra of the magnon mode in Sr_2IrO_4 under pressure were discussed briefly in Ref. 16. The spectra demonstrated in Fig. 4 cover a similar pressure range with a much higher signal-to-background ratio, leading to clearly revealed magnon profiles. We have measured low frequency magnetic excitations of Sr_2IrO_4 with the optical Raman technique up to 23.5 GPa. More detailed discussion of the magnetic behavior will be presented in future publications. In comparison with other high-pressure magnon studies in the literature,[15,17] our results have a significantly higher counting efficiency, primarily due to the use of both volume Bragg gratings and a microscope lens with a large numerical aperture. The high efficiency in measurement should significantly improve the

prospects of using Raman scattering to finely probe magnetism across pressure-induced quantum phase transitions and to explore spin-related quantum critical fluctuations.

ACKNOWLEDGMENTS

The authors thank D. Hsieh for the use of Sr_2IrO_4 single crystal samples. Y.F. acknowledges support from the Okinawa Institute of Science and Technology Graduate University (OIST), with subsidy funding from the Cabinet Office, Government of Japan. The authors also acknowledge the Mechanical Engineering and Microfabrication Support Section of OIST for technical support. The work at Caltech was supported by AFOSR Grant No. FA9550-20-1-0263.

DATA AVAILABILITY

The data that support the findings of this study are available from the corresponding author upon reasonable request.

REFERENCES

[1]I. Mirebeau, I. N. Goncharenko, P. Cadavez-Peres, S. T. Bramwell, M. J. P. Gingras, and J. S. Gardner, Nature **420**, 54 (2002).
[2]B. A. Frandsen, L. Liu, S. C. Cheung, Z. Guguchia, R. Khasanov, E. Morenzoni, T. J. S. Munsie, A. M. Hallas, M. N. Wilson, Y. Cai, G. M. Luke, B. Chen, W. Li, C. Jin, C. Ding, S. Guo, F. Ning, T. U. Ito, W. Higemoto, S. J. L. Billinge, S. Sakamoto, A. Fujimori, T. Murakami, H. Kageyama, J. A. Alonso, G. Kotliar, M. Imada, and Y. J. Uemura, Nat. Commun. **7**, 12519 (2016).
[3]Y. Wang, T. F. Rosenbaum, A. Palmer, Y. Ren, J.-W. Kim, D. Mandrus, and Y. Feng, Nat. Commun. **9**, 2953 (2018).
[4]Y. Wang, T. F. Rosenbaum, and Y. Feng, IUCrJ **6**, 507 (2019).
[5]W. Bi, J. Lim, G. Fabbris, J. Zhao, D. Haskel, E. E. Alp, M. Y. Hu, P. Chow, Y. Xiao, W. Xu, and J. S. Schilling, Phys. Rev. B **93**, 184424 (2016).
[6]E. Duman, M. Acet, E. F. Wassermann, J. P. Itié, F. Baudelet, O. Mathon, and S. Pascarelli, Phys. Rev. Lett. **94**, 075502 (2005).
[7]R. Loudon, Adv. Phys. **13**, 423 (1964).
[8]M. G. Cottam and D. J. Lockwood, *Light Scattering in Magnetic Solids* (John Wiley & Sons, 1986).
[9]T. P. Devereaux and R. Hackl, Rev. Mod. Phys. **79**, 175 (2007).
[10]A. Jayaraman, Rev. Mod. Phys. **55**, 65 (1983).
[11]F. D. Medina and W. B. Daniels, J. Chem. Phys. **64**, 150 (1976).
[12]S. Buchsbaum, R. L. Mills, and D. Schiferl, J. Phys. Chem. **88**, 2522 (1984).
[13]M. Lavagnini, H.-M. Eiter, L. Tassini, B. Muschler, R. Hackl, R. Monnier, J.-H. Chu, I. R. Fisher, and L. Degiorgi, Phys. Rev. B **81**, 081101(R) (2010).
[14]S. L. Gleason, Y. Gim, T. Byrum, A. Kogar, P. Abbamonte, E. Fradkin, G. J. MacDougall, D. J. Van Harlingen, X. Zhu, C. Petrovic, and S. L. Cooper, Phys. Rev. B **91**, 155124 (2015).
[15]S. Bettler, G. Simutis, G. Perren, D. Blosser, S. Gvasaliya, and A. Zheludev, Phys. Rev. B **96**, 174431 (2017).
[16]Y. Gim, Ph.D. dissertation (University of Illinois at Urbana-Champaign, 2018).
[17]S. Bettler, L. Stoppel, Z. Yan, S. Gvasaliya, and A. Zheludev, Phys. Rev. Res. **2**, 012010(R) (2020).
[18]Y. Feng, R. Jaramillo, J. Wang, Y. Ren, and T. F. Rosenbaum, Rev. Sci. Instrum. **81**, 041301 (2010).
[19]Y. Feng, D. M. Silevitch, and T. F. Rosenbaum, Rev. Sci. Instrum. **85**, 033901 (2014).
[20]Y. Feng, R. Jaramillo, G. Srajer, J. C. Lang, Z. Islam, M. S. Somayazulu, O. G. Shpyrko, J. J. Pluth, H.-K. Mao, E. D. Isaacs, G. Aeppli, and T. F. Rosenbaum, Phys. Rev. Lett. **99**, 137201 (2007).
[21]M. I. Eremets, *High Pressure Experimental Methods* (Oxford University Press, New York, 1996).
[22]K. Shimizu, H. Ishikawa, D. Takao, T. Yagi, and K. Amaya, Nature **419**, 597 (2002).
[23]R. Bini, L. Ulivi, J. Kreutz, and H. J. Jodl, J. Chem. Phys. **112**, 8522 (2000).
[24]Y. Gim, A. Sethi, Q. Zhao, J. F. Mitchell, G. Cao, and S. L. Cooper, Phys. Rev. B **93**, 024405 (2016).
[25]H. Gretarsson, J. Sauceda, N. H. Sung, M. Höppner, M. Minola, B. J. Kim, B. Keimer, and M. Le Tacon, Phys. Rev. B **96**, 115138 (2017).
[26]J. H. Burnett, Z. H. Levine, and E. L. Shirley, Phys. Rev. B **64**, 241102 (2001).
[27]A. R. Lang, Nature **213**, 248 (1967).